PHYSICAL REVIEW D **84,** 034503 (2011)

# Radiative transitions in charmonium from $N_f = 2$ twisted mass lattice QCD

Ying Chen,[1] De-Chuan Du,[2] Bao-Zhong Guo,[2] Ning Li,[2] Chuan Liu,[3,*] Hang Liu,[2] Yu-Bin Liu,[4] Jian-Ping Ma,[5] Xiang-Fei Meng,[6] Zhi-Yuan Niu,[2] and Jian-Bo Zhang[7]

(CLQCD Collaboration)

[1]*Institute of High Energy Physics, Chinese Academy of Sciences, Beijing 100049, People's Republic of China*
[2]*School of Physics, Peking University, Beijing 100871, People's Republic of China*
[3]*School of Physics and Center for High Energy Physics, Peking University, Beijing 100871, People's Republic of China*
[4]*School of Physics, Nankai University, Tianjin 300071, People's Republic of China*
[5]*Institute of Theoretical Physics, Chinese Academy of Sciences, Beijing 100080, People's Republic of China*
[6]*National supercomputer center, Tianjin, 300457, People's Republic of China*
[7]*Department of Physics, Zhejiang University, Hangzhou 310027, People's Republic of China*

(Received 18 April 2011; published 22 August 2011)

We present an exploratory study for charmonium radiative transitions: $J/\psi \to \eta_c\gamma$, $\chi_{c0} \to J/\Psi\gamma$, and $h_c \to \eta_c\gamma$ using $N_f = 2$ twisted-mass lattice QCD gauge configurations. The single-quark vector form factors for $\eta_c$ and $\chi_{c0}$ are also determined. The simulation is performed at a lattice spacing of $a = 0.067(2)$ fm and the lattice size is $32^3 \times 64$ with a pion mass of about 485 MeV. After extrapolation of lattice data at nonzero $Q^2$ to 0, we compare our results with previous quenched lattice results and the available experimental values.

DOI: 10.1103/PhysRevD.84.034503 PACS numbers: 12.38.Gc, 11.15.Ha

## I. INTRODUCTION

Charmonium physics plays an important and unique role in our knowledge of quantum chromodynamics (QCD), which is believed to be the fundamental theory for strong interactions. In some sense, it is comparable to the hydrogen atom for atomic physics, the basic theory of which being quantum electrodynamics (QED). However, charmonium physics is much more involved in the sense that, due to its intermediate energy scale and the special features of QCD, both perturbative and nonperturbative physics are present. It is therefore an ideal testing ground for our understanding of QCD from both perturbative and nonperturbative sides.

Radiative transitions among various charmonium states are particularly important in the study of charmonium physics. Most charmonium ground states lie below the open-charm ($D\bar{D}$) threshold which makes these states particularly interesting. Because of the suppression of the Okubo-Zweig-Iizuka (OZI) rule, these charmonium states usually have rather narrow widths. This makes their radiative transitions and radiative decays have significant branching ratios and be experimentally accessible. It is also believed to be the ideal hunting ground for exotic hadronic states like the glueballs whose existence is anticipated in QCD while its experimental signature remains obscure. Recently, the experimental interests have been revived with the upgrade for the BESIII experiment at BEPCII storage ring [1,2] which collects charmonium samples that are orders of magnitude larger than ever.

On the theoretical side, charmonium transitions have been studied using various methods. The physical process involves both electromagnetic (e.m.) and strong interactions, the former being perturbative in nature with the latter being nonperturbative. Therefore, nonperturbative lattice calculations are preferred. Radiative transitions of charmonia have been studied comprehensively in quenched lattice QCD for the normal ground state charmonia [3] and even for some excited and exotic ones [4]. However, an unquenched lattice study is still lacking. In this paper, we would like to pursue the feasibility of such a calculation using $N_f = 2$ dynamical twisted-mass fermion configurations generated by the European Twisted Mass Collaboration (ETMC). Twisted-mass fermions have been utilized successfully in various lattice QCD studies, see Refs. [5–17]. In this exploratory study, the calculation is performed at one value of lattice spacing [$a = 0.067(2)$ fm] [18]. We note, however, that the systematic uncertainties due to lattice artifacts are $O(a^2)$ with our discretization.

This paper is organized as follows: In Sec. II, we briefly describe the lattice setup for the calculation of the hadron matrix element from three-point correlation functions in the theory. In Sec. III, simulation details are provided and the results are presented. This includes the charmonium spectrum and the dispersion relations, the single-quark form factors for $\eta_c$, $\chi_{c0}$ and the radiative transition matrix elements responsible for $J/\Psi \to \eta_c\gamma$, $\chi_{c0} \to J/\Psi\gamma$, and $h_c \to \eta_c\gamma$. From these hadronic matrix elements that we

*Corresponding author.
liuchuan@pku.edu.cn

 

obtained in our lattice calculation, we compute the transition decay width for these channels which are then compared with experimental values and the quenched results. In Sec. IV we will summarize our results and conclude.

## II. THREE-POINT AND TWO-POINT CORRELATION FUNCTIONS

The lattice setup in this calculation is analogous to the vector form factor calculation of pions which has been studied extensively [19–25]. Here we will briefly review the general ideas involved.

The transitions among charmonium states are triggered by the electromagnetic interaction: $\mathcal{L}_{\rm int}^{\rm (e.m.)} = \int d^4x A^\mu(x) \times j_\mu^{\rm (e.m.)}(x)$ between the quark degrees of freedom and the photon field. Here $A^\mu(x)$ is the photon field and $j_\mu^{\rm (e.m.)}(x)$ is the electromagnetic vector current of the quarks. Since the electromagnetic interaction is weak, one can treat it perturbatively. This leads to the computation of the hadronic matrix element of the current operator between the initial ($|i\rangle$) and the final ($\langle f|$) charmonium states: $\langle f|j_\mu^{\rm (e.m.)}(x)|i\rangle$. We emphasize that, although the electromagnetic interaction is perturbative, the matrix element of the current between two hadronic states is in general nonperturbative. This is the quantity that we would like to compute using genuine nonperturbative methods like lattice QCD.

Within the framework of lattice QCD, charmonium states are realized by applying appropriate interpolating operators ($\mathcal{O}_1$ and $\mathcal{O}_2$ in the formula below) to the QCD vacuum $|\Omega\rangle$. Thus, the computation of the hadronic matrix element $\langle f|j_\mu^{\rm (e.m.)}(x)|i\rangle$ naturally leads to the following three-point function:

$$G_\mu(t_2, t; \mathbf{p}_2, \mathbf{p}_1) = \sum_{\mathbf{x}_2, \mathbf{x}} e^{-i\mathbf{p}_2\cdot\mathbf{x}_2} e^{+i\mathbf{q}\cdot\mathbf{x}} \langle\Omega|T\mathcal{O}_2(t_2, \mathbf{x}_2) \times j_\mu^{\rm (e.m.)}(t, \mathbf{x})\mathcal{O}_1^\dagger(0, \mathbf{0})|\Omega\rangle. \quad (1)$$

In this formula, interpolating operators which will create/annihilate the appropriate charmonium states are inserted at time slices $t = 0$ (the source operator) and $t = t_2$ (the sink operator), respectively. Local operators are used at the source and the sink. The sink operator is further Fourier transformed to acquire a definite three-momentum $\mathbf{p}_2$. The current insertion at time slice $t$ also carries a definite three-momentum $\mathbf{q}$. Momentum conservation then implies that the initial state also has a definite momentum $\mathbf{p}_1$ with $\mathbf{q} = \mathbf{p}_2 - \mathbf{p}_1$. Physically speaking, the three-point function defined above represents a process in which an initial charmonium state with three-momentum $\mathbf{p}_1$ created by $\mathcal{O}_1^\dagger$ makes an electromagnetic transition to the final charmonium state with three-momentum $\mathbf{p}_2$ annihilated by $\mathcal{O}_2$ while the three-momentum difference $\mathbf{q}$ is carried away by the photon.

Inserting a complete set of states between the electromagnetic current operator and the charmonium operators, one finds that, when $t_2 \gg t \gg 1$, the states with the lowest energy dominate the three-point function:

$$G_\mu(t_2, t; \mathbf{p}_2, \mathbf{p}_1) \xrightarrow{t_2\gg t\gg 1} \frac{e^{-E_2 t_2} e^{-(E_1 - E_2)t}}{4E_1(\mathbf{p}_1)E_2(\mathbf{p}_2)} \langle\Omega|\mathcal{O}_2|f(\mathbf{p}_2)\rangle\langle i(\mathbf{p}_1)|\mathcal{O}_1^\dagger|\Omega\rangle \times \langle f(\mathbf{p}_2)|j_\mu^{\rm (e.m.)}(0)|i(\mathbf{p}_1)\rangle. \quad (2)$$

Therefore, the desired hadronic matrix element $\langle f(\mathbf{p}_2)|j_\mu^{\rm (e.m.)}(0)|i(\mathbf{p}_1)\rangle$ can be obtained once the energies $E_1$, $E_2$ and the corresponding overlap matrix elements $\langle\Omega|\mathcal{O}_2|f(\mathbf{p}_2)\rangle$, $\langle i(\mathbf{p}_1)|\mathcal{O}_1^\dagger|\Omega\rangle$ are known, all of which can be obtained from corresponding two-point functions for the initial and final charmonium states.

For this purpose, two-point correlation functions for the interpolating operators $\mathcal{O}_i$ for $i = 1, 2$ are also computed in the simulation:

$$C_i(t, \mathbf{p}) \equiv \sum_{\mathbf{x}} e^{-i\mathbf{p}\cdot\mathbf{x}} \langle\Omega|\mathcal{O}_i(t, \mathbf{x})\mathcal{O}_i^\dagger(0, \mathbf{0})|\Omega\rangle \xrightarrow{t\gg 1} \frac{|Z_i(\mathbf{p})|^2}{E_i(\mathbf{p})} e^{-E_i(\mathbf{p})\cdot(T/2)} \cosh\left[E_i(\mathbf{p}) \cdot \left(\frac{T}{2} - t\right)\right], \quad (3)$$

where $Z_i(\mathbf{p}) = \langle\Omega|\mathcal{O}_i|N(\mathbf{p})\rangle$ is the corresponding overlap matrix element.

With the relevant two-point and three-point functions, the hadronic matrix element $\langle f(\mathbf{p}_2)|j_\mu^{\rm (e.m.)}(0)|i(\mathbf{p}_1)\rangle$ could be extracted using two methods: The first is to fit the two-point function Eq. (3) and three-point function Eq. (2) simultaneously. The second is to form an appropriate ratio from the two-point and three-point functions and extract the matrix element $\langle f(\mathbf{p}_2)|j_\mu^{\rm (e.m.)}(0)|i(\mathbf{p}_1)\rangle$ directly from the ratio. In this study, the second method is utilized and the relevant ratio is defined as

$$R_\mu(t) = \frac{G_\mu(t_2, t; \mathbf{p}_2, \mathbf{p}_1)}{C_2(t_2, \mathbf{p}_2)} \sqrt{\frac{C_1(t_2 - t, \mathbf{p}_1)C_2(t, \mathbf{p}_2)C_2(t_2, \mathbf{p}_2)}{C_2(t_2 - t, \mathbf{p}_2)C_1(t, \mathbf{p}_1)C_1(t_2, \mathbf{p}_1)}} \simeq \frac{\langle f(\mathbf{p}_2)|j_\mu^{\rm (e.m.)}(0)|i(\mathbf{p}_1)\rangle}{4\sqrt{E_2(\mathbf{p}_2)E_1(\mathbf{p}_1)}}, \quad (4)$$

where the second line becomes valid when $t_2 \gg t \gg 1$, assuming only the corresponding ground states dominate. In this case, $R_\mu(t)$ becomes independent of $t$ and fitting the ratio to a plateau behavior yields the desired hadronic matrix element $\langle f(\mathbf{p}_2)|j_\mu^{\rm (e.m.)}(0)|i(\mathbf{p}_1)\rangle$.

Because of different implementations for fermions on the lattice, the electromagnetic current operator $j_\mu^{\rm (e.m.)}(x)$ might take different forms as compared with its continuum counterpart. For Wilson-like fermions, like the twisted-mass fermions that we use in this study, one could use either the local current or the conserved current. The local current is simpler in form but it is not conserved on the lattice. It thus requires an additional multiplicative renormalization given by the factor $Z_V$, which of course can be

determined nonperturbatively [3]. The conserved current is slightly more complicated but due to its conservation, it does not need further renormalization, i.e. its multiplicative renormalization constant $Z_V \equiv 1$. In this work, we use the conserved current and the fact that $Z_V = 1$ is also verified numerically in our simulation.

In computing the three-point function defined in Eq. (2), various quark contributions arise. Since the electromagnetic current consists of contributions for all flavors of quarks, light flavors (i.e. $u$, $d$, and $s$ quarks) also contribute. Since our charmonium interpolating operators are formed only from charm quarks, the contribution from the light flavors can only occur through the so-called disconnected diagrams. The computation of these diagrams requires the light flavor quark propagators at basically all points on the lattice (the so-called all-to-all propagators). This is computationally extremely costly. Since the total electric charge of light quarks adds up to zero, one could argue that this contribution vanishes exactly in the flavor $SU(3)$ limit. In this study, these contributions are neglected as is the case for previous quenched studies [3]. Thus, we only need the charm quark contribution for the electromagnetic current which is proportional to the conserved current $j_\mu(x)$ on the lattice via $j_\mu^{(\mathrm{e.m.})}(x) = Q_c j_\mu(x)$ with $Q_c$ being the electric charge of the charm quark. The conserved current $j_\mu(x)$ for the twisted-mass quark is given by

$$j_\mu(x) = \bar{c}(x)\frac{\gamma_\mu - 1}{2}U_\mu(x)c(x+\mu) + \bar{c}(x+\mu)\frac{\gamma_\mu + 1}{2} \times U_\mu^\dagger(x)c(x). \tag{5}$$

When this current is inserted into the three-point function, disconnected diagrams due to the charm quark in principle can still arise. These are neglected in this study since charm quark is much heavier than the light quarks and they are also OZI suppressed. Therefore, within the approximations described above, we only have to compute the connected diagrams from the charm current which can be treated using the sequential source method [3,26].

## III. SIMULATION DETAILS

### A. The simulation setup for $N_f = 2$ twisted-mass fermions

Twisted-mass fermions at the maximal twist are utilized in our study with two degenerate light flavors in the sea. The framework of maximally twisted-mass fermions has been utilized in various studies of lattice QCD and are shown to be highly promising. It offers several advantages when tuned to maximal twist: (i) automatic $\mathcal{O}(a)$ improvement [27] is obtained when the bare untwisted quark mass is tuned to its critical value. Thus, only one parameter needs to be tuned. (ii) The determinant of the twisted-mass Dirac operator is strictly positive, protecting it against possible zero modes in the so-called exceptional configurations. (iii) It simplifies the operator mixing problem for renormalization.

In this study, gauge field configurations using $N_f = 2$ ($u$ and $d$ quark) twisted-mass fermion are utilized. Other quark flavors, namely the strange and charm quarks, are introduced as valence quarks. As discussed in Refs. [6,10,11,28], we implement nondegenerate valence quarks in the twisted-mass formulation by formally introducing a twisted doublet for each nondegenerate quark flavor. So, in the valence sector we introduce three twisted doublets, $(u, d)$, $(s, s')$, and $(c, c')$ with masses $\mu_l$, $\mu_s$, and $\mu_c$, respectively. Within each doublet, the two valence quarks are regularized in the physical basis with Wilson parameters of opposite signs ($r = -r' = 1$). The fermion action for the valence sector in the so-called "twisted basis" reads

$$\begin{aligned} S = {} & (\bar{\chi}_u, \bar{\chi}_d)(D_W + m_{\mathrm{crit}} + i\mu_l\gamma_5\tau_3)\begin{pmatrix}\chi_u \\ \chi_d\end{pmatrix} + (\bar{\chi}_s, \bar{\chi}_{s'}) \\ & \times (D_W + m_{\mathrm{crit}} + i\mu_s\gamma_5\tau_3)\begin{pmatrix}\chi_s \\ \chi_{s'}\end{pmatrix} + (\bar{\chi}_c, \bar{\chi}_{c'}) \\ & \times (D_W + m_{\mathrm{crit}} + i\mu_c\gamma_5\tau_3)\begin{pmatrix}\chi_c \\ \chi_{c'}\end{pmatrix}, \end{aligned} \tag{6}$$

where $D_W$ is the usual Wilson-Dirac operator, and $m_{\mathrm{crit}}$ is the critical quark mass which is predetermined from the simulation by ETMC. The relation between the fields in the twisted basis and the physical basis is as follows:

$$\begin{aligned} \begin{pmatrix}u \\ d\end{pmatrix} &= \exp(i\omega\gamma_5\tau_3/2)\begin{pmatrix}\chi_u \\ \chi_d\end{pmatrix}\begin{pmatrix}s \\ s'\end{pmatrix} \\ &= \exp(i\omega\gamma_5\tau_3/2)\begin{pmatrix}\chi_s \\ \chi_{s'}\end{pmatrix}\begin{pmatrix}c \\ c'\end{pmatrix} \\ &= \exp(i\omega\gamma_5\tau_3/2)\begin{pmatrix}\chi_c \\ \chi_{c'}\end{pmatrix}, \end{aligned} \tag{7}$$

where $\omega = \pi/2$ implements the full twist.

In this work, all computations are done using $N_f = 2$ twisted-mass fermion configurations at the lattice spacing of $a = 0.067(2)$ fm ($\beta = 4.05$) [18]. The size of the lattice is $32^3 \times 64$ so that the spatial extent of the lattice is about 2.14 fm, which is a safe value for charmonium physics. In the temporal direction, an antiperiodic boundary condition is applied for the quark field while a periodic boundary condition is utilized in all spatial directions. The simulation parameters for our study are summarized in Table I.

As for the charmonium states, we only need the valence charm quark. So we have adopted the Osterwalder-Seiler variant of the twisted-mass fermion [15,29]. In the physical basis, they read $\bar{c}\Gamma c$ and the corresponding form in twisted

TABLE I. Simulation parameters in this study.

| $L^3 * T$ | $\beta$ | $\kappa_c$ | $a$ [fm] | $a\mu$ | $m_\pi$ [MeV] | $N_{\mathrm{conf}}$ |
|---|---|---|---|---|---|---|
| $32^3 * 64$ | 4.05 | 0.15701 | 0.067(2) | 0.0080 | 485 | 201 |

TABLE II. Local interpolating fields for charmonium states studied in this work in both physical and twisted basis, $\bar{c}\Gamma c = \bar{\chi}_c\Gamma'\chi_c$. Also listed are the names of the corresponding particle and their $J^{PC}$ quantum numbers in the continuum.

| | $J/\psi$ | $\eta_c$ | $\chi_{c0}$ | $\chi_{c1}$ | $h_c$ |
|---|---|---|---|---|---|
| $\Gamma$ | $\gamma_i$ | $\gamma_5$ | 1 | $\gamma_i\gamma_5$ | $\sigma_{ij}$ |
| $\Gamma'$ | $\gamma_i$ | 1 | $\gamma_5$ | $\gamma_i\gamma_5$ | $\sigma_{0i}$ |
| $J^{PC}$ | $1^{--}$ | $0^{-+}$ | $0^{++}$ | $1^{++}$ | $1^{+-}$ |

basis $\bar{\chi}_c\Gamma'\chi_c$ can also be obtained easily. These are tabulated in Table II together with the possible $J^{PC}$ quantum numbers in the continuum and the names of the corresponding particle.[1]

Two-point functions are computed as usual for all charmonium states involved (those listed in Table II) in our calculation. Fitting these two-point functions yields the energy for the corresponding charmonium states, both with and without three-momentum. As for the three-point functions, since only connected diagrams involving charm propagators are needed, a sequential source method is utilized [26]. The results for the two-point and three-point functions are then employed to construct the relevant ratio defined in Eq. (4). For definiteness, we set $t_2 = 32$ in our simulations which makes the three-point function antisymmetric (for $j_{\mu=0}$) or symmetric (for $j_i$ with $i = 1, 2, 3$) [19] about the time slice $t_2 = 32$. In practice, we average the data from the two halves to improve statistics. All errors in this study are estimated using the conventional jackknife method.

### B. Charmonium spectrum and dispersion relations

Before computing the transition matrix element, the mass and the energy dispersion relations for the relevant charmonium states have to be verified. This is particularly important for our study due to the following reasons. Although charmonium spectrum has been studied extensively in quenched lattice QCD and the overall picture agrees reasonably well with the experiment, some quantities like the mass splitting between $\eta_c$ and $J/\Psi$ disagrees with the experimental value. It is widely believed that this discrepancy mainly originates from the quenched approximation. It is therefore useful to check, using unquenched twisted-mass configurations, whether this discrepancy can be resolved. Furthermore, although twisted-mass configurations have been used successfully to study the light flavors, using them on heavy charm quark needs some care. Being relatively heavy, the charm quark mass parameter $\mu_c a \sim 0.2$ in our study is not tiny. Of course, the good news from the maximally twisted-mass lattice QCD is that it is $\mathcal{O}(a)$ improved. Therefore, one would still hope to bring the lattice discretization errors under control. Another measure of the possible lattice artifacts is the charmonium mass, say the mass of the $\eta_c$ meson $m_{\eta_c}$ in lattice units. In our study, it turns out that $m_{\eta_c} a \sim 1$. For charmonium states with nonzero three-momentum, this number becomes even larger. Therefore, one should carefully verify that these possible lattice artifacts for the charmonium states are not out of control. Only after these reassurances can one possibly proceed to calculate transitions among charmonium states reliably. Since in this study only one lattice spacing is employed, this issue is particularly important. As we will illustrate below, in our simulation, most of these lattice artifacts are remedied by using the lattice dispersion relations for the charmonium states.

Following Eq. (3), the energy $E(\mathbf{p})$ for a particular charmonium state with three-momentum $\mathbf{p}$ can be obtained from the corresponding two-point function via

$$\cosh(E(\mathbf{p})) = \frac{C(\mathbf{p}; t-1) + C(\mathbf{p}; t+1)}{2C(\mathbf{p}; t)}. \tag{8}$$

The two-point function is symmetric about $t = T/2$. In real simulation we average the data from two halves about $t = T/2$ to improve statistics. For each channel, several three-momenta (including the zero three-momentum) have been computed. Different momentum modes that are related by lattice symmetries are averaged over.

The effective mass plateaus at zero three-momentum for the charmonium states studied in this work are illustrated in Fig. 1. These plateaus are found automatically by minimizing the $\chi^2$ per degree of freedom. From lower to higher values, the plateau corresponds to the charmonium state of $\eta_c$, $J/\Psi$, $\chi_{c0}$, $h_c$, and $\chi_{c1}$, respectively. It is seen that the effective mass values for $\eta_c$ and $J/\Psi$ have shown very clear and well-established plateau behavior, resulting in rather small statistical errors. We use the mass of $J/\Psi$ from our simulation to set the bare charm quark mass

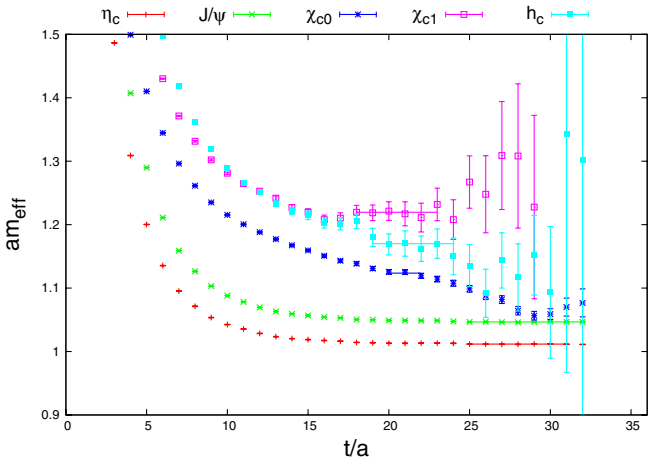


FIG. 1 (color online). Charmonium effective mass plateaus. From lower to higher values, the plateau corresponds to the charmonium state $\eta_c$, $J/\Psi$, $\chi_{c0}$, $h_c$, and $\chi_{c1}$, respectively.

[1]In the first row of the table, we list the names of the charmonium states where $\chi_{c0}$ and $\chi_{c1}$ are not to be confused with the charm quark field in the twisted basis.

parameter $\mu_c$. After some tuning, we find $a\mu_c \simeq 0.203$ roughly corresponds to the value that is consistent with the value quoted in the Particle Data Group (PDG). We then fix $\mu_c$ at this particular value for all our subsequent calculations. Since twisted-mass lattice QCD is $\mathcal{O}(a)$ improved, the anticipated cutoff effects induced by the charm quark mass is roughly $\mathcal{O}(a^2\mu_c^2)$, which is at a few percent level. This of course still needs further verification from measured physical quantities. The effective mass plateaus for other charmonium states ($\chi_{c0}$, $\chi_{c1}$, and $h_c$) are relatively noisy with larger statistical errors. The fitted effective mass values are collected in Table III which can be compared with the corresponding values from PDG.

Our lattice result suggests $m_{J/\Psi} - m_{\eta_c} = 104$ MeV, which is close to the PDG value of about 117 MeV. This is already an improvement over the quenched studies where the lattice results are typically away by dozens of MeV. This can be understood qualitatively as follows. The scale of lattice studies are set using long-distance quantities (static quark antiquark potential in quenched and $f_\pi$ for unquenched). However, the running coupling for the quenched gives a smaller coupling at the higher scale, say the charm scale which results in a smaller mass splitting than unquenched result. This remaining discrepancy might come from lattice artifacts (since we are simulating at a fixed lattice spacing without taking the continuum extrapolation) and/or from the fact that we have neglected annihilation diagrams for the charm quark in the two-point function, as estimated in Ref. [30]. One should bare in mind though that our calculation is done at one particular lattice spacing. Therefore, the estimate of the lattice errors should be viewed as qualitative in nature. This will also affect the value of charm quark mass as shown in Ref. [18].

To get a feeling about the size of the lattice artifacts for the charmonium states with nonvanishing three-momenta, we investigate the dispersion relations for $\eta_c$, $J/\Psi$, and $\chi_{c0}$ states. The energy $E(\mathbf{p})$ is obtained from the corresponding effective mass plateaus of the two-point functions with prescribed three-momentum. As said in the beginning of this subsection, since the charmonium states are relatively heavy in lattice units, the continuum dispersion relation $E^2 = m^2 + c^2\mathbf{p}^2$ may not be a good description, where $c$ is the speed of light which should be close to unity if lattice artifacts are small and the physical meson is weakly interacting. Indeed, our data suggest that the naive continuum dispersion relation is violated with the fitted value of $c^2$ substantially away from unity by as much as 12% even for $\eta_c$ and $J/\Psi$ states. However, we find that, if we utilize the standard lattice dispersion relation

$$4\sinh^2\left(\frac{E(\mathbf{p})}{2}\right) = 4\sinh^2\left(\frac{m}{2}\right) + Z \times 4\sum_i \sin^2\left(\frac{p_i}{2}\right), \quad (9)$$

which recovers the naive dispersion relation in the continuum limit, we could describe our data extremely well with the fitted values of $Z$ for $\eta_c$ and $J/\Psi$ rather close to unity.

The dispersion relations for $\eta_c$, $J/\Psi$, and $\chi_{c0}$ are illustrated in Figs. 2–4, respectively. We find that $Z_{\eta_c} = 1.063(8)$, $Z_{J/\Psi} = 1.056(7)$, and $Z_{\chi_{c0}} = 1.13(24)$, all of which are close to the anticipated value $Z \simeq 1$. The difference seems to be at the order of $\mathcal{O}((\mu_c a)^2) \sim 4\%$ as the naive estimate suggests. In evaluating the two-point function, thanks to the averaging of various $\mathbf{p}$ related by lattice

TABLE III. Charmonium effective mass [unit: MeV].

| | $\eta_c$ | $J/\psi$ | $\chi_{c0}$ | $\chi_{c1}$ | $h_c$ |
|---|---|---|---|---|---|
| Mass (this work) | 2997.4 | 3101.0 | 3329.1 | 3613.2 | 3466.8 |
| Error | 0.5 | 0.7 | 6.3 | 18.4 | 23.0 |
| PDG | 2980.3 | 3096.9 | 3414.7 | 3510.7 | 3525.9 |

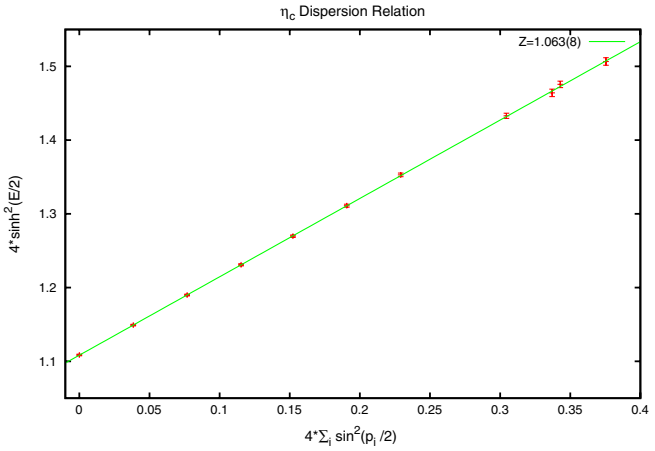


FIG. 2 (color online). The $\eta_c$ dispersion relation obtained from our calculation. Following the lattice dispersion relation (9), the quantity $4\sinh^2(\frac{E(\mathbf{p})}{2})$ (vertical axis) is plotted versus different values of $4\sum_i \sin^2(\frac{p_i}{2})$ (horizontal axis). The data points with errors are simulation results while the straight line is a linear fit according to Eq. (9) with the fitted value of $Z$ indicated in the upper right corner of the plot.

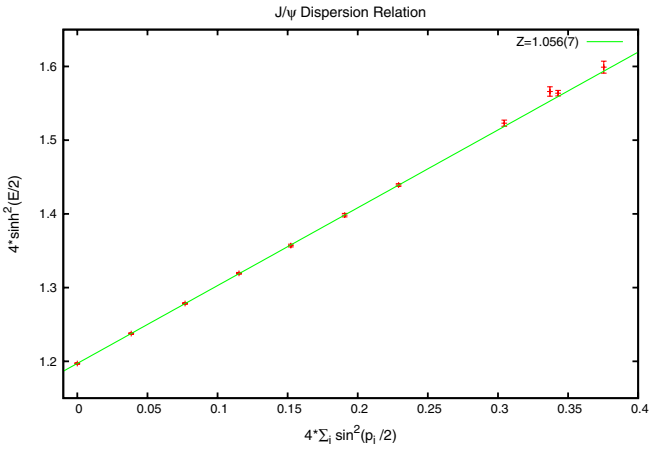


FIG. 3 (color online). The same as Fig. 2 but for $J/\Psi$.

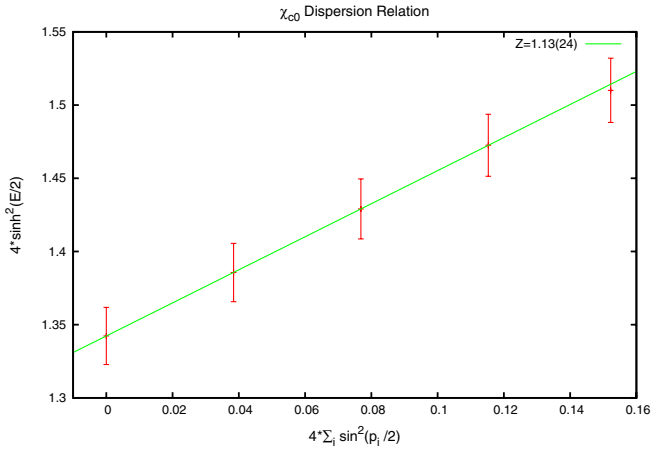


FIG. 4 (color online). The same as Fig. 2 but for $\chi_{c0}$.

symmetries, we get a very good dispersion relation even at $\mathbf{p}^2$ as large as $10\mathbf{p}^2_{\rm min}$, where $\mathbf{p}_{\rm min} = (100)$ [in unit of $(2\pi)/L$]is the minimal lattice momentum. It is also seen that, even at the largest three-momentum, the lattice dispersion relation still offers a very good description of the data. This gives us confidence that, at this particular lattice spacing that we are simulating, most of the lattice artifacts for the charmonium states are taken care of by using the lattice dispersion relation (9).

### C. Form factors for $\eta_c$ and $\chi_{c0}$

In the continuum, the hadronic matrix element $\langle\eta_c(\mathbf{p}_2)|j_\mu(0)|\eta_c(\mathbf{p}_1)\rangle$ may be parametrized by only one form factor $f(Q^2)$ as [3]

$$\langle\eta_c(\mathbf{p}_2)|j_\mu(0)|\eta_c(\mathbf{p}_1)\rangle \equiv f(Q^2)(p_1 + p_2)_\mu, \qquad (10)$$

where $Q^2 \equiv -(p_2 - p_1)^2$ is the square of four momentum transfer. This quantity is also called the single-quark elastic form factor in Ref. [31]. It is not a directly measurable quantity experimentally. But it is a quantity that can be computed in lattice simulations which can then be utilized to compare with similar results from models (see Ref. [31]). Note that this form automatically ensures the current conservation $\langle\eta_c(\mathbf{p}_2)|\partial^\mu j_\mu|\eta_c(\mathbf{p}_1)\rangle = 0$ since $q\cdot(p_1 + p_2) = (p_2 - p_1)\cdot(p_2 + p_1) = 0$. On a finite lattice, the partial derivatives are replaced by corresponding finite differences on the lattice. For the temporal components of the four-momenta, this amounts to replacing the continuum energy by its lattice counterpart: $(p_i)_0 \to 2\sinh(E_i/2)$. Note that similar modifications apply to some of the energy factors in Eq. (4). Of course, in principle the spatial components should also be modified according to the lattice dispersion relation (9). But since our three-momenta are relatively small in lattice units, this replacement does not make a significant change. For the temporal components, however, since $aE(\mathbf{p}) \sim 1$ for all charmonium states being studied, this modification is crucial. For example, according to Eq. (10), the form factor $f(Q^2)$ is a scalar function which is the same for all indices $\mu = 0, 1, 2, 3$. Only after using the modifications suggested by the lattice dispersion relation can we obtain consistent results for $f(Q^2)$ at different values $\mu$.

To obtain the desired hadronic matrix element $\langle\eta_c(\mathbf{p}_2)|j_\mu(0)|\eta_c(\mathbf{p}_1)\rangle$, we form the ratio defined in Eq. (4). This is done for the zero three-momentum case $\mathbf{p}_2 = (0, 0, 0)$ and for various nonvanishing three-momenta. In Figs. 5 and 6, we display the typical behaviors for $R_0(t)$ for $\mathbf{p}_2 = (0, 0, 0)$ and $\mathbf{p}_2 = (0, 0, 1)$, respectively. The plateaus are found automatically by minimizing the $\chi^2$ per degree of freedom. It is seen that clear plateau behaviors have been established from which the form factor $f(Q^2)$ can be extracted. We have checked that taking the temporal and spatial components of the current yields consistent results for $f(Q^2)$ although the results obtained from $\mu = 0$ [i.e. $R_0(t)$] gives smaller statistical errors, which we take as the final result for the form factor at that particular $Q^2$.

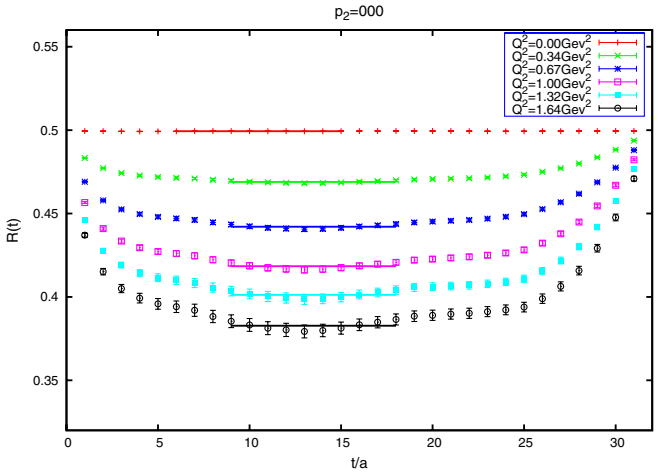


FIG. 5 (color online). The ratio $R_0(t)$ defined in Eq. (4) for $\eta_c$ with $\mathbf{p}_2 = (0, 0, 0)$.

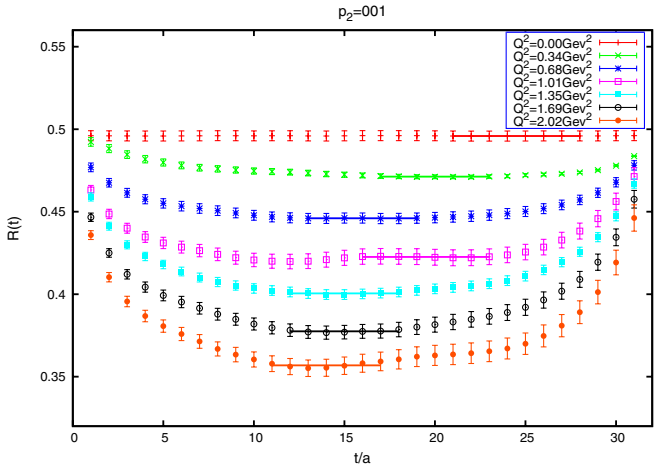


FIG. 6 (color online). The ratio $R_0(t)$ defined in Eq. (4) for $\eta_c$ with $\mathbf{p}_2 = (0, 0, 1)$.

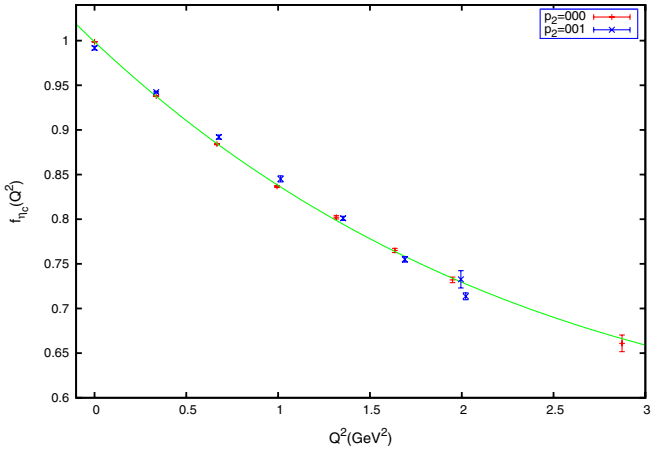


FIG. 7 (color online). The form factor $f(Q^2)$ for $\eta_c$ obtained from $\mathbf{p}_2 = (0, 0, 0)$ (red data points) and $\mathbf{p}_2 = (0, 0, 1)$ (blue data points). The curve is a fit for all the data using the functional form of Eq. (11).

The fitted values of $f(Q^2)$ obtained from the ratio are shown in Fig. 7 versus different values of $Q^2$ where two different types of symbols stand for $\mathbf{p}_2 = (0, 0, 0)$ and $\mathbf{p}_2 = (0, 0, 1)$, respectively. It is seen that the data obtained in the two cases tend to lie on a universal curve. Following Ref. [3], we fit the data for the form factor with the following function:

$$f(Q^2) = \exp\left[-\frac{Q^2}{16\beta^2}(1 + \alpha Q^2)\right]. \tag{11}$$

The fitted parameters turn out to be

$$\alpha = -0.096(6)\ \text{GeV}^{-2}, \qquad \beta = 567(2)\ \text{MeV}. \tag{12}$$

This value of $\beta$ is larger than the corresponding value 480(3) MeV obtained in the quenched approximation in Ref. [3], making the corresponding form factor obtained from our unquenched calculation "harder" (i.e. decays slower with increasing $Q^2$). The comparison of this form factor obtained from various phenomenological models with the corresponding quenched result has been addressed in Refs. [3,31]. It was noted that using the simple harmonic oscillator wave functions yields a harder form factor when compared with the quenched lattice result. In the quark model of Isgur-Scora-Grinstein-Wise [32], however, an extra factor $\kappa \simeq 0.7$ was introduced such that the form factor takes the form $f(Q^2) \sim \exp(-Q^2/(16\beta^2\kappa^2))$ near $Q^2 = 0$ which agrees with the *quenched* lattice result well, given a phenomenological value of $\beta \sim 710$ MeV. Since our unquenched lattice result suggests a harder behavior for the form factor than the quenched case, we find that, for the same value of $\beta$ taken in the model, a factor of $\kappa \simeq 0.8$ will make the model predictions in good agreement with our unquenched lattice results. One can define a squared mean charge radius $\sqrt{\langle r^2\rangle}$ with $\langle r^2\rangle$ given by

$$\langle r^2\rangle = -6\frac{d}{dQ^2}f(Q^2)\bigg|_{Q^2=0} = \frac{6}{16\beta^2}. \tag{13}$$

Our unquenched lattice result then yields $\sqrt{\langle r^2\rangle} = 0.213(1)$ fm which is smaller than the corresponding quenched value of 0.255(2) fm.

We should emphasize that both our study and the previous quenched study presented in Ref. [3] are performed at one value of lattice spacing, with different lattice regularization schemes which results in different size of the lattice artifacts. Therefore, although the estimated lattice artifacts are believed to be relatively small in both cases, the comparisons between the quenched results and our results should still be taken at the qualitative level.

Our unquenched result yields a harder behavior for the form factors which can be understood qualitatively. Physical scales on the lattice are usually set by some long-distance physical quantities, like the static quark antiquark potential in the quenched or the pion decay constant in the $N_f = 2$ twisted-mass lattice QCD. However, it is known that quenched lattice QCD did not reproduce the true QCD $\beta$ function due to the lack of the quark loops. In particular, when running from the lower energy scale up to the scale of charmonium physics, quenched lattice QCD gives a more weakened strong coupling constant than unquenched lattice QCD. This is believed to be the major reason for the discrepancy between the mass splitting of $J/\Psi$ and $\eta_c$ in quenched lattice QCD with the true experimental result. Therefore, unquenching the quarks will basically make the effective coupling constant stronger at charmonium scale when compared with the quenched case. This in turn gives a smaller charge radius for the unquenched case, in agreement with what we find in our calculation.

The hadronic matrix element $\langle\chi_{c0}(\mathbf{p}_2)|j_\mu(0)|\chi_{c0}(\mathbf{p}_1)\rangle$ for $\chi_{c0}$ has the same form of decomposition as that for $\eta_c$. The corresponding form factor is defined as in Eq. (10). In exactly the same manner, we can obtain the form factor $f(Q^2)$ for $\chi_{c0}$ except that we have only computed the case $\mathbf{p}_2 = (0, 0, 0)$. This is illustrated in Fig. 8. The data is fitted with the function

$$f(Q^2) = f(0)\exp\left[-\frac{Q^2}{16\beta^2}\right]. \tag{14}$$

The fit parameters are

$$f(0) = 1.0002(5), \qquad \beta = 510(16)\ \text{MeV}. \tag{15}$$

This value of $\beta$ is also larger than the quenched value of 393(12) MeV from Ref. [3] (i.e. the unquenched form factor is also harder than the quenched one). Note that our fitted value of $\beta$ for $\chi_{c0}$ is smaller than that for $\eta_c$ resulting in a larger charge radius for $\chi_{c0}$ when compared with that for $\eta_c$. This is consistent with the quark model picture since $\chi_{c0}$ in this model is a $L = 1$ state and the

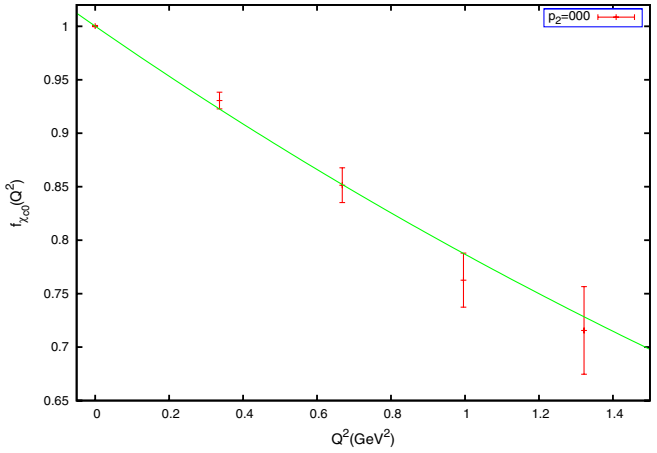


FIG. 8 (color online). The same as Fig. 7 except that the charmonium state is $\chi_{c0}$.

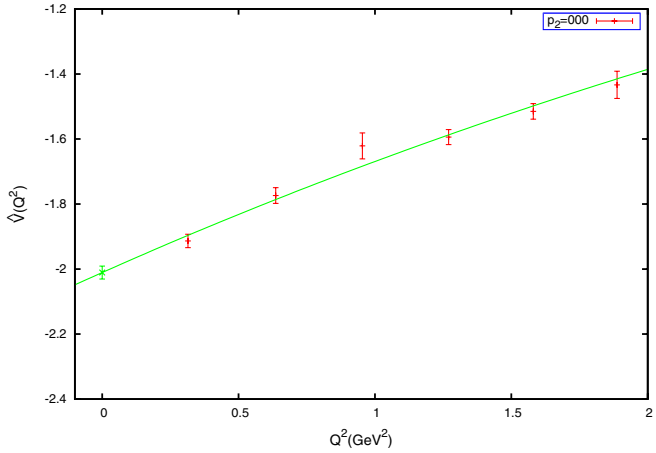


FIG. 9 (color online). The lattice results for the $J/\Psi \to \eta_c\gamma$ transition form factor $\hat{V}(Q^2)$. The curve is a fit using the function in Eq. (17). The fitted value of $\hat{V}(Q^2 = 0)$ is also shown at $Q^2 = 0$ together with its corresponding error.

charge radius is naturally larger due to the presence of the centrifugal potential.

Finally, we remark that, in cases of both $\eta_c$ and $\chi_{c0}$, although some data might have large errors at nonvanishing $Q^2$, the form factor as zero momentum transfer is always consistent with unity which is in fact a manifestation of the current conservation: $Z_V = 1$. Therefore, the conserved current requires no extra multiplicative renormalization as it should. This is verified numerically by our simulation data.

### D. $J/\Psi \to \eta_c\gamma$ transition

The matrix element $\langle \eta_c(\mathbf{p}_2)|j^\mu(0)|[J/\Psi]_r(\mathbf{p}_1)\rangle$ is responsible for the calculation of the $J/\Psi \to \eta_c\gamma$ transition rate. Here we use the index $r$ to designate the polarization of the initial $J/\Psi$ state whose polarization vector is denoted by $\epsilon_\gamma(\mathbf{p}_1, r)$. In the continuum, this matrix element can be decomposed as [3]

$$\langle \eta_c(\mathbf{p}_2)|j^\mu(0)|[J/\Psi]_r(\mathbf{p}_1)\rangle \equiv \frac{2V(Q^2)}{m_{\eta_c} + m_\Psi}\epsilon^{\mu\alpha\beta\gamma}p_{2\alpha}p_{1\beta}\epsilon_\gamma(\mathbf{p}_1, r). \quad (16)$$

Thus, the matrix element is characterized by one form factor $V(Q^2)$. By forming the appropriate ratio, relevant lattice results $\hat{V}(Q^2)$ are extracted from the plateaus of the ratios. The relation of $\hat{V}(Q^2)$ with its continuum counterpart $V(Q^2)$ is $V(Q^2) = 2 \times \frac{2}{3}e \times \hat{V}(Q^2)$, where the factor 2 comes from the quark and the antiquark while the factor $(2e/3)$ is due to the charge of the charm quark. The results for the transition form factor $\hat{V}(Q^2)$ thus obtained are illustrated in Fig. 9. Following Ref. [3], the data is fitted with the function

$$\hat{V}(Q^2) = \hat{V}(0)\exp\left[-\frac{Q^2}{16\beta^2}\right]. \quad (17)$$

The resulting fitted parameters we find are as follows:

$$\hat{V}(0) = -2.01(2), \qquad \beta = 580(19)\ \text{MeV}. \quad (18)$$

This is to be compared with similar results from previous quenched lattice study: $\hat{V}(0) = -1.85(4)$ and $\beta = 540(10)$ MeV in Ref. [3].

With the values of the transition form factor on the lattice, the $J/\Psi \to \eta_c\gamma$ decay width can be obtained:

$$\Gamma(J/\Psi \to \eta_c\gamma) = \alpha\frac{64}{27}\frac{|\mathbf{q}|^3}{(m_{\eta_c} + m_\Psi)^2}|\hat{V}(0)|^2, \quad (19)$$

where $\mathbf{q}$ is frame dependent. If we choose the frame in which the initial $J/\Psi$ is at rest, we have $|\mathbf{q}|^2 = (m_\Psi^2 - m_{\eta_c}^2)^2/(4m_\Psi^2)$. Substituting this into Eq. (19), we then get the $J/\Psi \to \eta_c\gamma$ decay width:

$$\Gamma_{m_{\text{phy}}} = 2.84(6)\ \text{KeV}, \qquad \Gamma_{m_{\text{lat}}} = 1.99(6)\ \text{KeV}, \quad (20)$$

where $\Gamma_{m_{\text{phy}}}$ denotes the result with physical mass values (e.g. values from PDG) are substituted into Eq. (19), while $\Gamma_{m_{\text{lat}}}$ stands for using the mass values computed from the lattice directly. This difference arises since our lattice results for the masses for $J/\Psi$ and $\eta_c$ in Sec. III B (see Table III) do not coincide with their experimental values exactly. Although our lattice value for the mass of the $J/\Psi$ is quite close and that for $\eta_c$ is also closer to the experimental value than the corresponding quenched value, the decay width turns out to be proportional to $(m_{J/\Psi} - m_{\eta_c})^3$ which magnifies the difference. Note that, for quenched lattice calculations, using different charmonium mass values makes a even bigger difference, as noted in Ref. [3]. The corresponding results are $\Gamma_{m_{\text{phy}}} = 2.57(11)\,\text{KeV}, \Gamma_{m_{\text{lat}}} = 1.61(7)\,\text{KeV}$. This is due to the fact that quenched lattice calculations yield a much smaller value for $m_{J/\Psi} - m_{\eta_c}$ when compared with the true experimental value. In our

unquenched study, however, we see that this difference is somewhat milder compared with the previous quenched situation. Both our lattice result and the previous quenched result for this quantity are to be compared with the value $\Gamma_{\rm PDG} = 1.58(38)$ KeV quoted by the PDG. Note that the PDG value is an average of CLEO result and the Crystal Ball result, the former being 1.92(30) KeV which is closer to our lattice result while the latter from Crystal Ball being 1.18(33) KeV, smaller than lattice results.

### E. $\chi_{c0} \to J/\Psi\gamma$ transition

In the continuum, this transition matrix element has the following decomposition [3]:

$$\langle S(\mathbf{p}_S)|j^\mu(0)|V(\mathbf{p}_V, r)\rangle = \Omega^{-1}(Q^2)\Big(E_1(Q^2)[\Omega(Q^2)\epsilon^\mu(\mathbf{p}_V, r) - \epsilon(\mathbf{p}_V, r)\cdot p_S(p_V^\mu p_V\cdot p_S - m_V^2 p_S^\mu)] + \frac{C_1(Q^2)}{\sqrt{q^2}} m_V \epsilon(\mathbf{p}_V, r)\cdot p_S[p_V\cdot p_S(p_V + p_S)^\mu - m_S^2 p_V^\mu - m_V^2 p_S^\mu]\Big) \tag{21}$$

with $\Omega(Q^2) = (p_V\cdot p_S)^2 - m_V^2 m_S^2$. Therefore, the hadronic matrix element is characterized by two form factors $E_1(Q^2)$ and $C_1(Q^2)$. At the physical photon point with $Q^2 = 0$, only the former contributes.

The form factor $E_1(Q^2)$ can be obtained by following a similar process as the other form factors. We can always choose some combinations of $p_V$, $p_S$ such that

$$\langle S(\mathbf{p}_S)|j^\mu(0)|V(\mathbf{p}_V, r)\rangle \propto E_1(Q^2).$$

The final lattice results for $\hat{E}_1(Q^2)$ are shown in Fig. 10. We then use the following form

$$\hat{E}_1(Q^2) = \hat{E}_1(0)\left(1 + \frac{Q^2}{\rho^2}\right)\exp\left[-\frac{Q^2}{16\beta^2}\right], \tag{22}$$

to fit the data [3]. The fitted parameters we obtain are

$$a\hat{E}_1(0) = -0.1699(51), \qquad \rho = 871(85)\ \text{MeV}, \qquad \beta = 451(62)\ \text{MeV}. \tag{23}$$

The fitted value of $\hat{E}_1(0)$ at $Q^2 = 0$ is also indicated in Fig. 10 together with its error. These results are to be compared with similar results from previous quenched lattice study [3]: $\beta = 542(35)$ MeV and $\rho = 1.08(13)$ GeV.

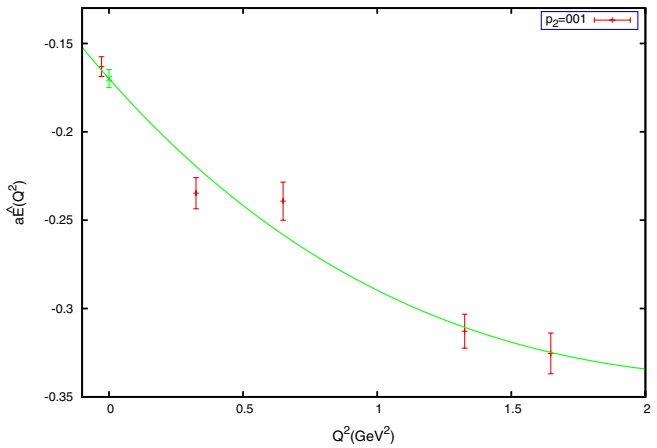


FIG. 10 (color online). $\chi_{c0} \to J/\Psi\gamma$ transition form factor $\hat{E}_1(Q^2)$ obtained from our simulation. The curve is a fit according to Eq. (22). The fitted value of $\hat{E}_1(Q^2 = 0)$ is also indicated at $Q^2 = 0$ with its error.

At the physical photon point $Q^2 = 0$, the decay width for this radiative transition is given by

$$\Gamma(\chi_{c0} \to J/\Psi\gamma) = \alpha\frac{16}{9}\frac{|\mathbf{q}|}{m_{\chi_{c0}}^2}|\hat{E}_1(0)|^2, \tag{24}$$

where $\hat{E}_1$ is related to $E_1$ by

$$E_1(Q^2) = 2\times\tfrac{2}{3}e\times\hat{E}_1(Q^2).$$

Substituting our lattice result for $\hat{E}_1(0)$, we then can get the decay width in physical unit:

$$\Gamma_{m_{\rm phy}} = 85(7)\ \text{KeV}, \qquad \Gamma_{m_{\rm lat}} = 65(4)\ \text{KeV} \tag{25}$$

which is to be compared with the quenched lattice result of $\Gamma_{m_{\rm phy}} = 232(41)$ KeV and $\Gamma_{m_{\rm lat}} = 288(60)$ KeV. It is seen that our unquenched result for this decay width is substantially smaller than their quenched values. The value for this quantity quoted by the PDG is given by $\Gamma_{\rm PDG} = 119(11)$ KeV, which lies in between the quenched and unquenched results.

### F. $h_c \to \eta_c\gamma$ transition

The form factor decomposition for this process is identical to Eq. (21). However, the signal for the state $h_c$ is much noisier. It turns out that we could only get reasonable signal with $\mathbf{p}_{h_c} = 000$. In order to get various values of $Q^2$, we vary the values of $\mathbf{q}$ and $\mathbf{p}_{\eta_c}$ simultaneously such that $h_c$ is always at rest.

The form factor we obtain is illustrated in Fig. 11. We fit the data with a functional form [3]:

$$\hat{E}_1(Q^2) = \hat{E}_1(0)\exp\left[-\frac{Q^2}{16\beta^2}\right], \tag{26}$$

and the fitted parameters come out to be

$$a\hat{E}_1(0) = -0.39(1), \qquad \beta = 440(23)\ \text{MeV}. \tag{27}$$

The fitted value of $\hat{E}_1(0)$ is also shown in Fig. 11 at $Q^2 = 0$ together with the corresponding error. These numbers are

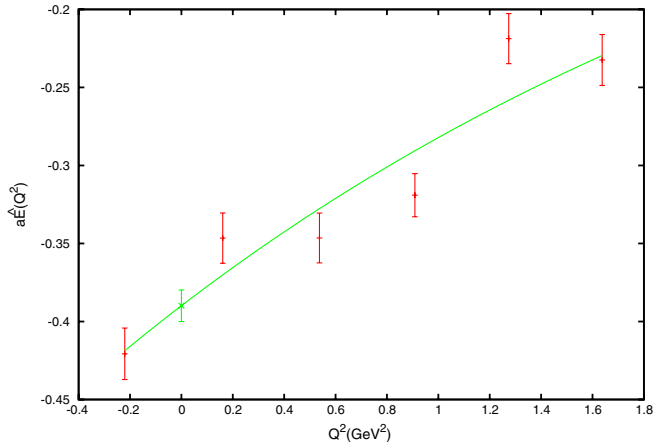


FIG. 11 (color online). The $h_c \to \eta_c\gamma$ transition form factor $\hat{E}_1(Q^2)$ obtained from our calculation (the data points). The curve is a fit using Eq. (26). Also shown at $Q^2 = 0$ is the fitted value of $\hat{E}_1(0)$ together with its error.

to be compared with the corresponding quenched result of $\beta = 689(133)$ MeV [3].

The physical decay width for the transition is given by

$$\Gamma(h_c \to \eta_c\gamma) = \alpha \frac{16}{27} \frac{|\mathbf{q}|}{m_{h_c}^2} |\hat{E}_1(0)|^2. \tag{28}$$

With our lattice result for $\hat{E}_1(0)$ substituted in, we find

$$\Gamma_{m_{\rm phy}} = 234(12)\ \text{KeV}, \qquad \Gamma_{m_{\rm lat}} = 210(13)\ \text{KeV}. \tag{29}$$

The corresponding quenched lattice values are $\Gamma_{m_{\rm phy}} = 601(55)$ KeV and $\Gamma_{m_{\rm lat}} = 663(132)$ KeV, both of which are about a factor of 3 larger than our unquenched result, though the errors are somewhat large. The lattice results for this decay can now be compared with the recent measurement at BESIII [33]. The total width for $h_c$ and the corresponding branching ratio for the radiative transition are found to be

$$\Gamma^{\rm tot}_{\rm exp} = 730 \pm 450 \pm 280\ \text{KeV},$$
$$B(h_c \to \eta_c\gamma) = (54.3 \pm 6.7 \pm 5.2)\%,$$

where the first error is statistical and the second is systematic. If we multiply the central values for the above two quantities and add the errors in quadrature, we find the decay width $\Gamma(h_c \to \eta_c\gamma) = 396(294)$ KeV, which could be compared with our lattice result. The agreement within a large error is seen although improvements from both experiment and lattice calculations are required to cut down the large uncertainties for this quantity.

## IV. SUMMARY AND CONCLUSIONS

In this exploratory study, we calculate the form factors for some of the ground state charmonia and their radiative transitions using unquenched $N_f = 2$ twisted-mass fermions. The $s$ and $c$ quarks are quenched which are incorporated via a twisted doublet for each nondegenerate quark flavor in the valence sector. Our study focuses on the form factors for $\eta_c$, $\chi_{c0}$ and the $J/\Psi \to \eta_c\gamma$, $\chi_{c0} \to J/\Psi\gamma$, $h_c \to \eta_c\gamma$ radiative transitions. The mass spectrum and dispersion relations for these charmonium states are first examined. Good agreement of the computed spectrum with the experiment is found. It is also verified that, by using lattice dispersion relations instead of the naive continuum ones, the lattice artifacts for these charmonium states are well under control. By computing various appropriate ratios of the three-point functions to the two-point functions, hadronic matrix elements for these transitions are obtained at various of $Q^2$. Using the parametrized form in terms of relevant form factors, we obtain the lattice results for the relevant form factors and the radiative decay widths for these channels. Our results are summarized in Table IV which are to be compared with those obtained in previous quenched lattice studies and experimental values.

Although some quantities from our unquenched study turn out to be comparable with the quenched results, quite a

TABLE IV. Summary of the results obtained in this work. Also listed are the corresponding results from quenched lattice QCD [3]. Experimental values or values from PDG are also listed whenever available.

| Fitted parameter $\beta$ [MeV] for form factors | | |
|---|---|---|
| | $\eta_c$ | $\chi_{c0}$ |
| This work | 567(2) | 510(16) |
| Ref. [3] | 480(3) | 393(12) |

| $\Gamma_{m_{\rm phy}}/\Gamma_{m_{\rm lat}}$ [KeV] for transitions | | | |
|---|---|---|---|
| | $J/\Psi \to \eta_c\gamma$ | $\chi_{c0} \to J/\Psi\gamma$ | $h_c \to \eta_c\gamma$ |
| PDG | 1.58(38) | 119(11) | 396(294) |
| This work | 2.84(6)/1.99(6) | 85(7)/65(4) | 234(12)/210(13) |
| Ref. [3] | 2.57(11)/1.61(7) | 232(41)/288(60) | 601(55)/663(132) |

number of the results still differ substantially, as is seen from Table IV. For example, for the form factors of $\eta_c$ and $\chi_{c0}$ a harder behavior (a larger value of $\beta$ hence a smaller charge radius) than the quenched result is found. As for the decay width for $J/\Psi \to \eta_c\gamma$, a value larger than the quenched result is obtained. Because of the improvement of the mass splitting for the charmonium in unquenched study, the discrepancy between the results using the physical mass and the lattice computed mass is somewhat narrowed, although the value is still larger than the value quoted by PDG. For the decay width of $\chi_{c0} \to J/\Psi\gamma$, a value smaller than the PDG value (and also the quenched result) is obtained. As for the $h_c \to \eta_c\gamma$ transition, the signal is noisy and our unquenched result is much smaller than the quenched value with a large statistical uncertainty. It is still compatible with the recently measured value at BESIII which also has a large error. To get better signals for this channel, variational methods or smearing techniques might be necessary which will be investigated in the future.

In this preliminary study, we simulate at only one lattice spacing and sea quark mass, and no chiral nor continuum extrapolation is made. The physics involved in this study mainly concerns the heavy flavor part of the theory which should not be sensitive to the pion mass. As for the lattice artifacts, we argued that, thanks to the automatic $\mathcal{O}(a)$ improvement, the lattice artifacts is under control. Indeed, by using the lattice dispersion relations, we verified that all charmonium states that we studied exhibit controlled lattice errors in their dispersion relations of about a few percent, which is roughly at the order of $(\mu_c a)^2$ for our simulation. Of course, to get a full control of the lattice errors, the calculation needs to be done on several lattice spacings and continuum limit has to be taken. With the experience gained in this study, it would be better and also possible to study charmonium radiative transitions in a more systematic manner (more lattice spacings, more pion mass values, etc.) using unquenched lattice QCD. It is also tempting to perform similar studies with the $N_f = 2 + 1 + 1$ dynamical twisted-mass fermion. Given the promising experimental status of BESIII at BEPCII, the unquenched lattice studies on charmonium transitions will certainly be an interesting project to pursue in the future.

## ACKNOWLEDGMENTS

The numerical computations for this project was performed on the Magic Cube at Shanghai Supercomputer Center and on Tianhe-1A at National Supercomputing Center in Tianjin. We thank the ETMC for allowing us to use their gauge field configurations and part of their packages. We thank Dr. X. Feng, K. Jansen, and M. Wagner for valuable discussions. This work is supported in part by the National Science Foundation of Chian (NSFC) under Projects No. 10835002, No. 11021092, No. 10675101, No. 11075167, and No. 10975076.

[1] M. Ablikim *et al.* (BESIII Collaboration), Nucl. Instrum. Methods Phys. Res., Sect. A **614**, 345 (2010).
[2] Special issue on physics at bes-iii, edited by K. T. Chao and Y. Wang [Int. J. Mod. Phys. A **24**, 1 (2009)].
[3] J. J. Dudek, R. G. Edwards, and D. G. Richards, Phys. Rev. D **73**, 074507 (2006).
[4] J. J. Dudek, R. G. Edwards, and C. Thomas, Phys. Rev. D **79**, 094504 (2009).
[5] Roberto Frezzotti, Pietro Antonio Grassi, Stefan Sint, and Peter Weisz, J. High Energy Phys. 08 (2001) 058.
[6] R. Frezzotti and G. C. Rossi, J. High Energy Phys. 10 (2004) 070.
[7] A. Shindler, Phys. Rep. **461**, 37 (2008).
[8] Ph. Boucaud *et al.* (ETM Collaboration) Phys. Lett. B **650**, 304 (2007).
[9] Ph. Boucaud *et al.* (ETM Collaboration) Comput. Phys. Commun. **179**, 695 (2008).
[10] B. Blossier *et al.* (ETM Collaboration) J. High Energy Phys. 04 (2008) 020.
[11] B. Blossier *et al.* (ETM Collaboration) J. High Energy Phys. 07 (2009) 043.
[12] R. Baron *et al.* (ETM Collaboration), J. High Energy Phys. 06 (2010) 111.
[13] R. Baron *et al.* (ETM Collaboration), J. High Energy Phys. 08 (2010) 097.
[14] C. Alexandrou *et al.* (ETM Collaboration), Phys. Rev. D **78**, 014509 (2008).
[15] C. Alexandrou *et al.* (ETM Collaboration), Phys. Rev. D **80**, 114503 (2009).
[16] Karl Jansen, Andrea Shindler, Carsten Urbach, and Ines Wetzorke, Phys. Lett. B **586**, 432 (2004).
[17] Stefan Sint, arXiv:hep-lat/0702008.
[18] B. Blossier *et al.*, Phys. Rev. D **82**, 114513 (2010).
[19] D. Brömmel *et al.*, Eur. Phys. J. C **51**, 335 (2007).
[20] J. N. Hedditch *et al.*, Phys. Rev. D **75**, 094504 (2007).
[21] T. Draper *et al.*, Nucl. Phys. **B318**, 319 (1989).
[22] J. M. Flynn *et al.*, J. High Energy Phys. 05 (2007) 016.
[23] P. A. Boyle *et al.*, J. High Energy Phys. 08 (2008) 086.
[24] Stefano Capitani, Christof Gattringer, and C. B. Lang, Phys. Rev. D **73**, 034505 (2006).
[25] R. Frezzotti, V. Lubicz, and S. Simula, Phys. Rev. D **79**, 074506 (2009).
[26] F. D. R. Bonnet, R. G. Edwards, G. T. Fleming, R. Lewis, and D. G. Richards, Phys. Rev. D **72**, 054506 (2005).
[27] R. Frezzotti and G. C. Rossi, J. High Energy Phys. 08 (2004) 007.

[28] Abdou M. Abdel-Rehim, Randy Lewis, R. M. Woloshyn, and Jackson M. S. Wu, Phys. Rev. D **74**, 014507 (2006).
[29] K. Osterwalder and E. Seiler, Ann. Phys. (N.Y.) **110**, 440 (1978).
[30] L. Levkova and C. DeTar, Phys. Rev. D **83**, 074504 (2011).
[31] Olga Lakhina and Eric S. Swanson, Phys. Rev. D **74**, 014012 (2006).
[32] Nathan Isgur, Daryl Scora, Benjamin Grinstein, and Mark B. Wise, Phys. Rev. D **39**, 799 (1989).
[33] The BESIII Collaboration, Phys. Rev. Lett. **104**, 132002 (2010).